Irwin, P. G. J., Fletcher, L. N., Read, P. L., de Pater, I., Orton, G. S., Teanby, N. A., & Davis, G. R. (2016). Spectral analysis of Uranus' 2014 bright storm with VLT/SINFONI. Icarus, 264, 72-89. DOI: 10.1016/j.icarus.2015.09.010

Spectral analysis of Uranus' 2014 bright storm with VLT/SINFONI

P. G. J. Irwin, L.N. Fletcher, P.L. Read, D.Tice

Department of Physics, University of Oxford, Parks Rd, Oxford OX1 3PU, UK.

irwin@atm.ox.ac.uk

I. de Pater

University of California, Berkeley, CA 94720, USA.

G.S. Orton

Jet Propulsion Laboratory, California Institute of Technology, 4800 Oak Grove Drive, Pasadena, CA 91109, USA.

N.A. Teanby

School of Earth Sciences, University of Bristol, Wills Memorial Building, Queens Road, Bristol, BS8 1RJ, UK

and

G.R. Davis

Square Kilometre Array Organisation, Jodrell Bank Observatory, Lower Withington Macclesfield, Cheshire, SK11 9DL, UK

Received _____; accepted _____

Submitted to Icarus

ABSTRACT

An extremely bright storm system observed in Uranus' atmosphere by amateur observers in September 2014 triggered an international campaign to observe this feature with many telescopes across the world. Observations of the storm system in the near infrared were acquired in October and November 2014 with SINFONI on ESO's Very Large Telescope (VLT) in Chile. SINFONI is an Integral Field Unit spectrometer returning 64×64 pixel images with 2048 wavelengths and uses adaptive optics. Image cubes in the H-band (1.43 – 1.87 μm) were obtained at spatial resolutions of $\sim 0.1''$per pixel.

The observations show that the centre of the storm feature shifts markedly with increasing altitude, moving in the retrograde direction and slightly poleward with increasing altitude. We also see a faint 'tail' of more reflective material to the immediate south of the storm, which again trails in the retrograde direction. The observed spectra were analysed with the radiative transfer and retrieval code, NEMESIS (Irwin et al., JSQRT 109, 1136, 2008). We find that the storm is well-modelled with a two main cloud components. The deep component is due to a brightening and increase in altitude of the main tropospheric cloud deck at 2 – 3 bars, while the upper component of the feature was modelled as being due to a vertical extension of the upper tropospheric cloud, based at 1.23 bar and assumed to be composed of methane ice. We also found this cloud to be responsible for the faint 'tail' seen to the feature's south and the brighter polar 'hood' seen in all observations polewards of $\sim 45°$N.

During the twelve days between our sets of observations the higher-altitude component of the feature was observed to have brightened significantly and moved to even higher altitudes, while the deeper component faded.

Subject headings: planets and satellites: atmospheres — planets and satellites: individual (Uranus)

1. Introduction

Although NASA's Voyager 2 spacecraft found Uranus to have a relatively featureless atmosphere during its fly-by of the planet in 1986, improved ground-based observations with ever-larger telescopes employing adaptive optics techniques have revealed the atmosphere of Uranus to be much more active and exotic than that seen by Voyager 2. In addition to larger telescopes and better imaging, a new class of instruments, Integral Field Unit (IFU) spectrometers, have become available, such as the SINFONI instrument at the European Southern Observatory's (ESO) Very Large Telescope (VLT), the NIFS instrument at Gemini-North, and the OSIRIS instrument at Keck II. Such instruments can simultaneously map planets like Uranus at thousands of wavelengths with spectral resolving powers in excess of $R = \lambda/\Delta\lambda = 1000$.

Since the mid 1990s several discrete clouds were seen in Uranus' atmosphere, generally at mid-latitudes, which became more frequent in the years leading up to the planet's northern spring equinox in 2007 (e.g. Sromovsky et al. 2007, 2009). Since equinox, Uranus continued to remain dynamically active, although overall cloud activity decreased. A notable exception to this was the detection of a bright spot near 25°N in November 2011 (Sromovsky et al. 2012).

Uranus cloud observations obtained with the Keck Telescope in August 2014 (de Pater et al. 2015) revealed an amazingly active Uranus; numerous cloud features were observed, amongst them the brightest cloud ever seen at a wavelength of 2.2 μm; this cloud ('Br' in their nomenclature) was seen at a latitude of $\sim$ 15.5°N. These observations triggered a campaign by amateur astronomers and shortly thereafter a very bright cloud was observed in September 2014. Both from tracking the position of this feature and its latitude, it was discovered to have evolved not from the brightest 'Br' feature observed by de Pater et al. (2015), but from a smaller feature at a higher latitude ($\sim$ 33°N), 'Feature 2' in de Pater et

al.'s nomenclature. This feature was identified as the deepest atmospheric feature seen with the Keck telescope in August 2014, at a pressure of near 2 bar. It also had an intriguing tail trailing in the retrograde direction. The fact that the cloud had been observed by amateurs sparked huge international interest amongst the professional planetary astronomy community and a number of Directors Discretionary Time (DDT) proposals were submitted to HST, Gemini, and VLT. Here we report the results of VLT/SINFONI DDT observations of Uranus made on October 31^{st} and November 11^{th} 2014.

2. Observations

To observe the cloud seen by the amateur astronomers (i.e., 'Feature 2' seen by de Pater et al. (2015)) observations of Uranus were made with the SINFONI instrument at the European Southern Observatory (ESO) Very Large Telescope (VLT) in La Paranal, Chile. SINFONI is an Integral Field spectrograph that can make use of adaptive optics to yield a spatial resolution of typically $0.1''$. Each one of SINFONI's 32 slitlets is imaged onto 64 pixels of the detector, giving 64×32 individual spectra, each with 2048 wavelengths, which are usually doubled in the cross-slit-direction to give 64×64 pixel 'cubes'. SINFONI has three pixel scale settings: $0.25''$, $0.1''$and $0.025''$giving Instantaneous Fields of View (IFOV) of $8''\times$ $8''$, $3''\times$ $3''$and $0.8''\times$ $0.8''$. Uranus was observed on October 31^{st} and November 11^{th} 2014 using the $0.1''$pixel scale and the H–grism, which has a spectral resolution of $R = \lambda/\Delta\lambda \sim 3000$. Two sets of observations (Table 1) were made per night, spaced by a couple of hours, to allow the cloud to be observed at more than one emission angle.

The data were reduced with the ESO VLT SINFONI pipeline, but correction for the stellar absorption features of the telluric standard star was made using the Spextool (Cushing et al. 2004) package *xtellcor-general*, which uses the method of Vacca et al. (2003). Photometric correction was achieved by integrating the observations of the A0

standard stars (HD212874 or HD210780) across the entire FOV, using the quoted 2MASS (Cutri et al. 2003) H-magnitudes of 8.917 and 8.255, respectively, and the 2MASS H-filter profiles. Geometric registration was done manually and planetocentric latitudes were assumed throughout. We also corrected for the airmass difference between the planet and standard star spectra.

Figure 1 shows a typical reflectance spectrum of Uranus as measured by IRTF/SpeX[1], together with the pressure level at which the transmission to space is 0.5 for a cloud-free atmosphere, assuming the standard atmospheric profile described in the next section. The main absorption features seen in Uranus' near-IR spectrum are formed by gaseous methane. At wavelengths of strong methane absorption sunlight cannot penetrate very far and thus any light we see must have been reflected from hazes in the stratosphere. Conversely, in regions of weak absorption sunlight can penetrate to be reflected from clouds at the deepest levels. Hence, as Fig.1 shows, such spectra allow us to probe the cloud density over a wide pressure range. In this paper, we present many false-colour plots, which show the distribution of deep, intermediate and high clouds/hazes. To generate these false-colour plots, we formed selected spectral averages to emulate filters targetting specific altitude levels. To map the deepest clouds we only use wavelengths where the transmission to space exceeds 0.5 at the 4-bar level. We shall call this the 'F4.0' filter. To map the intermediate clouds we choose only those wavelengths where the transmission to space is **less** than 0.5 at the 1.5-bar level ('F1.5' filter). To map the highest clouds we choose only those wavelengths where the transmission to space is less than 0.5 at the 0.4-bar level ('F0.4' filter). The wavelengths covered by these three 'filters' in the 1.47 – 1.71 μm range are shown in Fig.1. The appearance of Uranus recorded from 01:42 – 02:17 on October 31st 2014, using the 0.1″pixel scale in these three 'filters' is shown in the top row of Fig.2. The bottom row

[1]http://irtfweb.ifa.hawaii.edu/ spex/IRTF_Spectral_Library/

shows the differences between these images, highlighting the cloud density at low and medium altitudes (the F0.4 map already shows the cloud density at high altitudes), and also shows the aspect of Uranus at the time of observation. Figure 3 presents a false colour representation of these images, together with those observed at the other times listed in Table 1 and shows the distribution of low, medium and high altitude clouds/hazes.

Although the observations on 11^{th} November are slightly less well spatially resolved than those observed on 31^{st} October, a number of key points are immediately clear from both sets of observations: 1) the centre of the cloud at the deepest levels is consistently to the left (i.e. in the prograde direction) and slightly below (i.e. to the south of) the intermediate clouds; 2) the intermediate level clouds are brighter on 11^{th} November 2014, suggesting that clouds at this level have thickened and/or become more reflective in the two weeks since 31^{st} October; 3) to the south and right (retrograde direction) of the storm cloud appears a faint 'tail' of brighter material, also seen by de Pater et al. (2015), running roughly along a line of constant latitude (this is more easily seen in the continuum image of Fig.2); and 4) the storm (which resides at a latitude of 34.5°N) sits in a darker than average belt, lying between a medium-bright equatorial region and a significantly brighter 'hood' polewards of 40 – 50°N. Observations on both nights also show very faint clouds 'shadowing' the main features $\sim 60°$ longitude away in the retrograde direction, but it is difficult to discern much from these features in these observations.

The images shown in Fig.3 are mosaicked (2×2 mosaics with a 5^{th} frame centred on the disc) averages over a time span of roughly one hour, during which Uranus' rotates significantly. To capture a less rotationally distorted view, albeit at the expense of increased noise, Fig.4 shows the best individual frames targeting the storm in each average. Here we see the same key features and the reduced rotational smear is obvious.

The apparent change in intermediate level cloud density suggested by these observations

could possibly be due to differences in radiometric calibration between the two sets of observations. However, Fig.5 shows the individual wavelength-selected images used to make up the false colour image of the second observation on this date, and here we can see that the intermediate-level clouds really are brighter relative to the background disc brightness. Furthermore, we can see traces of the cloud in the upper-level F0.4 image (i.e. where transmission to space at the 0.4-bar level is less than 0.5), showing that the intermediate-level cloud is not only thicker, but higher as well. Finally, the observations on 11^{th} November clearly have lower spatial resolution than the 31^{st} October images, which should have the effect of lowering the brightness of pixels containing storm features, by blurring their contribution into neighbouring pixels, rather than raising the brightness as is apparent here.

3. Radiative Transfer and Retrieval Analysis

To analyse these data, the spectra in each pixel were first smoothed to an intermediate resolution, similar to that of the IRTF-SpeX instrument with a triangular-shaped instrument function with Full Width Half Maximum (FWHM) = 0.002 μm, giving a spectral resolution of $R \sim 775$. Although this sacrificed spectral resolution, it greatly increased our computation speeds and improved the signal-to-noise (SNR) ratio. This choice was justified by our previous high spectral resolution analysis of Uranus spectra (Irwin et al. 2012). From this analysis we concluded that, for cloud parameter retrievals, the lower IRTF-SpeX resolution was the best compromise between computational efficiency, vertical resolution and SNR.

The temperature and abundance profile assumed in this study was the same as that used by Irwin et al. (2015). The temperature profile was based on the 'F1' profile determined Sromovsky et al. (2011) with the helium volume mixing ratio set to 0.116 at

altitudes of negligible methane abundance, assuming 0.04% mole fraction of neon and a deep CH_4 mole fraction of 4%, which Karkoschka and Tomasko (2009) found to be most appropriate for latitudes equatorwards of 45°N,S.

These data were analysed using methane line data from the WKMC-80K line database (Campargue et al. 2012) in the same way as described by Irwin et al. (2012). The spectra were fitted with the NEMESIS (Irwin et al. 2008) radiative transfer and retrieval code, using a correlated-k radiative transfer model (Lacis and Oinas 1991) and methane k-tables derived from the WKMC-80K line data, assuming the IRTF-SpeX triangular instrument function with FWHM = 0.002 μm. These k-tables were computed using the hydrogen-broadened methane line shape of Hartmann et al. (2002) (suitable for atmospheres where H_2 is the main constituent) and have a line wing cut-off of 350 cm^{-1}, which we previously found to give good fits to our Uranus and Neptune Gemini/NIFS observations (Irwin et al. 2012). For this k-table, a CH_3D/CH_4 ratio of 3.6×10^{-4}, determined for Uranus by de Bergh et al. (1986), was assumed. Although Irwin et al. (2012) revised this value downwards to 2.9×10^{-4}, the effect on cloud retrievals at IRTF/SpeX resolution is not significant. For H_2 – H_2 and H_2 – He collision-induced absorption (CIA) we used the coefficients of Borysow (1991, 1992) and Zheng and Borysow (1995). An equilibrium ortho/para-H_2 ratio was assumed at all altitudes and latitudes. Although Conrath et al. (1998) and Fouchet et al. (2003) show that the ortho/para-H_2 ratio actually varies quite significantly with both altitude and latitude, the effect on the spectra in this wavelength band is insignificant. In addition to H_2 – H_2 and H_2 – He CIA, H_2 – CH_4 and CH_4 – CH_4 collision-induced absorption was also included (Borysow and Frommhold 1986, 1987) as was Rayleigh scattering by the air molecules themselves. The reference solar spectrum of Fiorenza and Formisano (2005) was used to simulate the solar flux.

To analyse these spectra we used a similar cloud model to that described by Sromovsky et al. (2011), which Irwin et al. (2015) found to give a good fit to IRTF/SpeX observations. This model has three thin clouds: a lower tropospheric cloud (LTC) based at 5 bar, a middle tropospheric cloud (MTC) based at around 2 – 3 bar, and an upper tropospheric cloud (UTC), assumed to be methane, based at around 1.2 bar. Higher in the atmosphere are two haze layers: a tropospheric haze (TH) extending between 0.9 and 0.1 bar, and a stratospheric haze (SH) extending between 0.1 and 0.01 bar. In these retrievals, we assumed that the bright storm clouds we see are convective methane ice clouds. To model these, we fixed the UTC to the methane condensation level, using methane refractive indices to model the scattering properties. However, instead of assuming this cloud was vertically thin, we allowed it to be vertically extended, described by a variable fractional scale height. While this model provided a good fit to the observations, the cloud occasionally extended beyond the tropopause, which was considered unphysical and also led to excessive reflectance in regions of strong methane absorption. Hence, we introduced an additional parameterisation to force the methane cloud density to reduce to zero at the tropopause level (at 0.1bar) with a tuneable degree of steepness governed by a pressure-dependent multiplicative factor: $1.0 - \exp(-((\log(p) - \log(0.1))/\alpha)^2)$, where the parameter α was fitted by the retrieval model and p is the pressure (in bar). Although it is usually assumed that, as on Earth, the tropopause acts like a sort of like a lid, de Pater et al. (2014) argue that for Neptune, material in vortices may ascend through the tropopause to higher levels since the temperature-pressure profile is so isothermal in this region. Since the temperature-pressure profile of Uranus is estimated to be even more isothermal in the tropopause region, it is possible that the tropospheric 'lid' constraint could also be broken at certain locations in Uranus' atmosphere. However, for the storm cloud considered here, there is very little trace at stratospheric latitudes, which suggests the vigour of this convective outbreak is not as strong as those occurring in Neptune's atmosphere.

As in the analysis of Irwin et al. (2015), we made use of a novel retrieval technique where, in addition to the cloud opacity and vertical position parameters, the imaginary refractive index spectrum of the cloud particles is retrieved. This can then be used in a Kramers-Kronig analysis to compute self-consistent extinction cross-section, single-scattering albedo and phase function spectra using Mie scattering, with the adjustment that we approximated the phase functions with combined Henyey-Greenstein functions. This adjustment was to eliminate phase function features peculiar to purely spherical particles, such as the 'glory' and 'rainbow', which are unlikely to be present for Uranian condensates, which are all predicted to be solid phase and thus almost certainly not spherical. To analyse these VLT Uranus spectra we adopted the same approach as Irwin et al. (2015) for the middle tropospheric cloud (MTC) and tropospheric haze (TH) particles, assuming *a priori* mean radii of 1.0 and 0.1 μm (with variance 0.05) respectively, and *a priori* refractive indices $1.4 + 0.001i$ at all wavelengths. When performing the Kramers-Kronig analysis, the real part of the refractive index was set to 1.4 at a wavelength of 1.6 μm. As assumed by Irwin et al. (2015), the scattering properties of the LTC were set to those empirically derived for the lower cloud by Tice et al. (2013), while we used the methane refractive indices of Martonchik et al. (1994) for the UTC. The spectral properties of the SH were those described by Sromovsky et al. (2011). Irwin et al. (2015) found that the complex refractive index spectrum of the TH was only loosely constrained by our H-band observations and hence, in the interests of computation time, the refractive index spectrum of the TH was left as *a priori*.

To demonstrate the suitability of this model, we initially analysed the 1^{st} set of observations recorded on 31^{st} October and picked three points: 1) a region well away from the storm at the same latitude, 2) the centre of the deeper cloud feature, and 3) the centre of the upper cloud feature. These points are indicated in Fig.3. Figure 6 shows the fit we achieve with this model at Point 1. As can be seen the quality of fit is extremely good.

Note that the error bars indicated include the estimated forward-modelling error employed by Tice et al. (2013) to account for discrepancies between the modelled and fitted spectra arising from remaining discrepancies in the line data and forward radiative transfer model. Figure 7 compares all three measured spectra in both linear and log space. Points 2 and 3 have higher radiances at 1.57 μm, but Point 3 (centre of upper cloud feature) has the highest radiance in the methane absorption band from 1.6 to 1.7 μm, indicating that the cloud lies at higher altitudes. Figure 8 compares the vertical cloud profiles derived in the three test cases, while Fig. 9 shows the retrieved refractive index spectrum of the MTC, which was found to be equivalent for all the points, and is very similar to that derived from IRTF/SpeX spectra by Irwin et al. (2015). Figure 8 shows in detail how the vertical cloud profile varies between the three points. In case 1 the methane UTC is retrieved to be vertically thin, as it is assumed to be on the Sromovsky et al. (2011) model. However, in case 2 it can be seen to be considerably vertically extended, and in case 3 easily reaches the tropopause at 0.1 bar, where its abundance is reduced to zero by the additional α cut-off parameter. The χ^2/n values listed in Figure 7 indicates that the fit is good for all three spectra, but to make this absolutely clear Fig. 10 shows our fit in case 3, which is our worst-fitting case, demonstrating that we fit the observations very well with this model.

Having tested our model on three individual cases, we ran our retrieval model over a wider region of the storm feature, covering the storm cloud itself and also the trailing cloud feature. The region covered by this wide-area retrieval is indicated in Fig.3. Our fitted radiance maps (at continuum and methane absorbing wavelengths) are shown in Fig.11, while our fitted cloud parameters are shown in Fig.12. Note, that since this is an average of several individual frames, artefacts are apparent at the joins between them. This is particularly clear at pixels with x-value 7 and 30 and thus features in this position are not real. Figure 12 suggests that the deep cloud feature is formed at the main cloud deck (i.e. the MTC, panel (c)), while the opacity of the UTC (i.e. methane cloud, panel (d)) is

responsible for the trailing feature, and also the polar 'hood'. The higher component of the feature is seen to caused by the increased fractional scale height of the UTC (panel (e)), which leads to this cloud reaching very high altitudes in a small region near $x = 10$, and so needs to be limited to zero at the tropopause by the cut-off parameter α, which is seen to locally peak at this point (panel (f)). The 'trailing feature' to the right of the main cloud can be seen to be caused by a thickening of the UTC (i.e. the methane cloud), which can also be seen to be responsible for the brighter reflectance of the polar 'hood'.

Broader features in the hazes are considered to be the result of 'aliasing' effects. This aliasing arises from the fact that over the H–band wavelength range, the spectral signature of changing the TH or SH opacity is rather similar and cannot easily be discriminated from each other (or from the UTC fractional scale height, when this parameter has a large value). The indistinguishability seen here at H–band only is in contrast to studies where a wider range of wavelengths can be considered (Irwin et al. 2015; Sromovsky et al. 2011), where the differing scattering spectra of these components allows them to be separated. Hence, the opacity maps of the TH and SH are included here only for completeness and are not particularly physically meaningful. Note that the effect of the SH at these wavelengths is particularly small as can be inferred from the opacity at 1.6 μm which is only $\sim 10^{-5}$. The opacity of the TH is somewhat larger, however, ($\sim 10^{-3}$ at 1.6 μm) and there is a greater effect on the modelled spectrum. In particular, we found that when the fractional scale height of the UTC was large, its spectral signature was almost indistinguishable from the TH. This did not cause any problems here, where the UTC fractional scale height was mostly small, but in our retrievals for the 11^{th} November, reported later, where larger values for this parameter were inferred, this led to instability, requiring us to fix the TH opacity at its mean value seen here of 0.002 at 1.6 μm. To test whether fixing the TH opacity would affect the modelling these data we repeated these 31^{st} October retrievals with the TH opacity fixed to 0.002. We found that the retrieved spatial distributions of

the LTC, MTC and UTC parameters were the same as those shown here, which supports our initial assumption that these transient opacity variations arise mostly from variations in the optical thickness of the MTC and UTC, and also the vertical extent of the UTC, i.e. the methane cloud. To determine reliable maps of the SH and TH opacity would require observations covering a wider wavelength range.

To test the effect of rotational 'smearing', the best individual frame (frame 17) recorded in the 1^{st} set of observations of October 31^{st} was analysed with our retrieval model, focussing this time just on the storm region and the trailing cloud feature. The longitudinal spreading was reduced, as expected, but at the expense of a slightly poorer spatial resolution in the vertical direction (caused by not adding several dithered frames leading to lower signal-to-noise ratios). We do not present these retrievals here, but from them the same general conclusions were drawn: 1) the deep part of the storm cloud is formed by a brightening and rising of the MTC; 2) the upper part of the cloud is caused by a vertical extension of the UTC, which rises so high that the cloud density has to be forced to zero at the tropopause; and 3) the 'trailing' feature caused by a slight thickening of the UTC, as is the polar 'hood'.

We then applied our retrieval model to the observations made on 11^{th} November 2014. We chose the 2^{nd} set as this had the storm closer to the centre of the disc and thus the geometry matched more closely the 31^{st} October retrievals. The results are presented in Figs. 13 and 14. Here we see the same shift in the centre of the storm as we go from spectral regions of low to high methane absorption, but in this observation, taken nearly two weeks after those on 31^{st} October, we can see that the cloud is notably thicker at higher altitudes, but less thick at the base, making the 'yellowish' component in Fig. 3 brighter and the 'reddish' component dimmer. Once again we find that the deeper part of the cloud coincides with a brightening and rising of the MTC, while the upper part of the cloud coincides with

increased opacity of the UTC, together with much higher fractional scale heights than were seen on 31^{st} October and also much higher cut-off rates. To see what this means in terms of cloud density as a function of height, Fig. 15 compares the measured spectra at three points, indicated in Fig.3: 1) a spot away from the storm; 2) a point in the centre of the deep cloud; and 3) a point in the centre of the upper component of the cloud. In Fig. 15 we can see the same trend in reflectivity spectra as seen on 31^{st} October, although the spectrum from the deep cloud centre is noticeably dimmer, while both the deep- and intermediate-component cloud pixels are generally brighter at wavelengths of strong methane absorption. Figure 16 compares the retrieved cloud profiles from these three points. Comparing Fig.16 with Fig.8 we can see that the UTC is generally thicker and that the retrieval is trying to shift the main position up from the fixed base at 1.23 bars. NEMESIS achieves this by retrieving a fractional scale height in the cloud greater than 1.0, which means that the cloud density falls less quickly with height than pressure and thus the relative abundance of cloud increases. However, such an increase cannot continue indefinitely or we would end up with significant amounts of the UTC in the stratosphere, which is not thought to be physically likely, and which would also lead to significant reflectance at the wavelengths of strongest methane absorption, which is not seen. Hence, NEMESIS increases the tropopause cut-off parameter to bring the number density more steadily back to zero at the tropopause (0.1 bar). This considerably extended UTC makes the signature of the UTC and TH virtually inseparable and initial retrievals became unstable. Hence, in the retrievals presented here the opacity of the TH was fixed to the mean value determined from the 31^{st} October observations of 0.002. Finally, although the final χ^2/n values look large, especially at pixels in the centre of the upper cloud component, we actually achieve a very good fit as can be seen in Fig.17. The large values of χ^2/n seen actually have more to do with the very low estimated forward model error of Tice et al. (2013) at 1.63 – 1.65 μm than inherent model inadequacies, although the model does have difficulty in fitting the 1.65 to 1.67 μm region, suggesting

there is too much cloud at upper levels in the model. This may partly have been caused by our fixing the TH opacity in this retrieval to ensure stability, but more likely indicates that our chosen three-parameter model of the vertical distribution of UTC opacity is not sophisticated enough and requires further refining.

4. Discussion

The centre of the cloud observed is at a latitude (planetocentric) of 34.5°. At this latitude, the zonal wind strength on Uranus is estimated to be ≈ 100m/s in the prograde direction (Hammel et al. 2001) and this is a region of maximum horizontal wind-shear (i.e. maximum du/dy). This may help to confine the feature into a 'vortex' and explain its longevity and that of other cloud features that regularly appear at this latitude. From the temperature fields determined by Voyager 2 (Conrath et al. 1998) Uranus' winds are estimated to be decaying with height and more recent ground based observations of Uranus' thermal structure suggest there has been no ostensible change since the Voyager 2 observations (Orton et al. 2015). From its morphology, the cloud appears to be a convective event, formed deep in the atmosphere, which then 'bubbles up' into the high atmosphere where the winds are slightly lower, causing the cloud column to become sheared with height in the direction we see. We were initially concerned that this vertical wind-shear would soon disrupt this cloud and spread it along this latitude band, rather as was seen for Saturn's northern springtime storm disturbance, or 'Great White Spot', observed in 2010/2011 (Sánchez-Lavega et al. 2011; Fletcher et al. 2011, 2012). However, this latitude band (30 – 45°N) is also one where there is a minimum in upper tropospheric temperatures and thus $\partial T/\partial y$ approaches zero. From the Thermal Wind Equation we expect $\partial u/\partial p \propto \partial T/\partial y$ and thus the vertical wind shear should be at a minimum at this latitude, which would also help to explain the cloud's longevity. Assuming the feature is indeed a convective event, confined

by the zonal winds as described, the 'tail' of material immediately to the south, which is seen in these observations and also the Keck observations of 'Feature 2' of de Pater et al. (2015), would appear to be cloud material that is somehow escaping from this vortex and trailing along in the slower moving zonal winds immediately to the feature's south.

An alternative interpretation of this feature is that we are instead seeing some sort of wave feature, where air rises and falls through the disturbance as it flows zonally (perhaps akin to the process of clouds formed by orographic uplift), and the wave propagation characteristics lead to the disturbance's vertical structure. Although we keep the UTC fixed at 1.23 bar, we allowed the base pressure of the MTC to vary and we can see that this moves to lower pressures in the deep cloud centre, which is consistent with this picture. It is also possible that allowing the base of the UTC to move would improve the fit to the observed spectra, but if this cloud is really a methane condensation cloud that would imply either a reduction in the methane mole fraction from 4% to something lower, or instead a local increase in temperature, which intriguingly, might be consistent with the latent heat released by the apparent thick cloud condensation. From its size (roughly 3,500 km in diameter) the feature is too large to be explained simply by gravity waves, although it is possibly the manifestation of a Rossby wave. However, if this were the case we would expect to see a semi-regular train of such features along this latitude band, which is difficult to discern, although it is conceivable that the faint features seen $\sim 60^\circ$ longitude away in the retrograde direction might be a manifestation of such a wave. Unfortunately, our observations do not have sufficient SNR to probe these fainter features more fully and on balance we believe this cloud to be caused by a localised convective event, which evolved during our observation sequence, becoming more vertically extended. Assuming it is a convective cloud feature it is interesting to consider how such an event might be triggered. At the high temperatures in Uranus' deep atmosphere we expect the ratio between the ortho-H_2 and para-H_2 isomers to be 3:1, equivalent to a para-H_2 fraction (f_p) of 25%. At

lower temperatures, and given sufficient time to come to equilibrium the para-H_2 fraction (f_p) rises. Hence, regions of low f_p can be considered to be regions where air has risen from below faster than the para-H_2 isomer can be converted into ortho-H_2. Together with being the coldest upper tropospheric region, the 30 – 45°N latitude range is also one with the lowest para-H_2 fraction compared with the rest of the northern hemisphere (Orton et al. 2015), which suggests that this region is one where material is rising up from below. However, unlike other examples of low-f_p regions on the Giant Planets, such as the Equatorial Zones on both Jupiter and Saturn, where a thick cloudy zone is formed, it appears that on Uranus, this upwelling is somehow temporarily 'trapped' below the main cloud deck at 2 – 3 bar, before being occasionally released into large convective features such as the cloud feature observed here. In other words, it is possible that there might be a build up of Convective Available Potential Energy (CAPE) beneath the cloud deck, followed by occasional 'eruptions', rather like Saturn's storm or Jupiter's SEB revival. Such events could be seasonally triggered and it is intriguing that these large storms are being seen in the springtime hemispheres of both Uranus and Saturn. It is possible that the increased seasonal warming changes the stability of the overlying troposphere with regards to moist convective penetration on both planets, potentially triggering these events.

5. Conclusions

Our VLT/SINFONI observations of the bright storm cloud detected in Uranus' atmosphere in the autumn of 2014 contain unique information on the vertical structure and temporal evolution of this cloud feature, allowing much finer vertical resolution than can be achieved by filter-imaging observations alone, albeit at slightly poorer spatial resolution. We analysed these observations with our radiative transfer and retrieval code, NEMESIS using a version of the Uranus cloud scheme proposed by Sromovsky et al. (2011), modified

to include a vertically extended Upper Tropospheric Cloud (UTC). During the period of observations we found that the storm feature was well modelled by variations of two of the main component clouds: 1) a brightening and rising of the main Middle Tropospheric Cloud (MTC) deck at the 2 – 3 bar level; and 2) a thickening and vertical extension of the Upper Tropospheric Cloud (UTC), based at 1.23 bar and assumed to be composed of methane ice. Our observations show that the centre of storm clouds shifts markedly with increasing altitude, with the top of the cloud centred significantly further upwind than the base. From its morphology the features appears to be a convective cloud, and we find that the latitude band in which the feature sits (30 – 40°N) may be particularly conducive to the longevity of such features as it is a region of maximum latitudinal, but minimum vertical wind shear.

Between 31^{st} October and 11^{th} November 2014 we found that the UTC component thickened significantly and became more vertically extended, while the MTC component faded. The 'tail' feature seen to the south of the main cloud in these observations, and also by de Pater et al. (2015), was accounted for by a thickening of the UTC, which was reproduced for the brighter polar 'hood' seen in all observations polewards of ~ 45°N.

Our simple three-component model (optical depth, fractional scale height, cut-off parameter) of the UTC was found to give good results everywhere, except in the very middle of the upper cloud, especially in the second set of observations on 11^{th} November 2014. It would appear that in these cases the model requires refinement, which will be the subject of further work. This further work will also incorporate the higher zenith-angle observations taken of the same cloud on both nights, which will improve still more the vertical resolution. We find that to place meaningful constraints on the opacity variations of the tropical and stratospheric hazes requires simultaneous measurements over a wider spectral range of the same feature in order to disentangle the contributions of the different layers in the Uranus vertical cloud scheme of Sromovsky et al. (2011). Such measurements

will have to wait until the next bright cloud of this type is spotted in Uranus' atmosphere.

Finally, these observations show the efficacy of modern Integral Field Unit spectrometers such as VLT/SINFONI in probing the vertical cloud structure of Uranus and the other giant planets. Although Uranus is long past its equinox in 2007, its atmosphere remains highly active. It will be of great interest to see how this activity evolves and whether there will be any further convective outbreaks as Uranus' north pole swings towards the Sun over the next decade until it reaches northern winter solstice in 2028. By that stage, it will presumably have reverted to the subdued, quiescent state observed by Voyager 2 during its encounter with Uranus at southern summer solstice in 1986.

6. Acknowledgements

We are very grateful to our VLT/SINFONI support astronomer George Hau who helped us hugely in designing these observations at short notice and executing them. Leigh Fletcher was supported by a Royal Society Research Fellowship at the University of Oxford. Glenn Orton was supported by a grant from NASA to the Jet Propulsion Laboratory, California Institute of Technology. The VLT/SINFONI observations were performed at the European Southern Observatory (ESO), Proposal 294.C-5004, as part of the Director's Discretionary Time (DDT).

Facilities: VLT (SINFONI).

REFERENCES

Borysow, A., 1991. Modeling of collision-induced infrared absorption spectra of H_2 – H_2 pairs in the fundamental band at temperatures from 20 to 300 K. Icarus 92, 273 – 279.

Borysow, A., 1992. New model of collision-induced infrared absorption spectra of H_2 – He pairs in the 2 – 2.5 μm range at temperatures from 20 to 300 K – An update. Icarus 96, 169 – 175.

Borysow, A., Frommhold, L., 1986. Theoretical collision-induced rototranslational absorption spectra for the outer planets H_2 – CH_4 pairs. Astrophys. J. 304, 849 – 865.

Borysow, A., Frommhold, L., 1987. Collision induced rototranslational absorption spectra of CH_4 – CH_4 pairs at temperatures from 50 to 300 K. Astrophys. J. 318, 940 – 943.

de Bergh, C., Lutz, B.L., Owen, T., Brault, J., Chauville, J., 1986. Monodeuterated methane in the outer Solar System. II. Its detection on Uranus at 1.6 μm. ApJ, 311, 501 – 510.

Campargue, A., Wang, L., Mondelain, D., Kassi, S., Bzard, B., Lellouch, E., Coustenis, A., de Bergh, C., Hirtzig, M., Drossart, P., 2012. An empirical line list for methane in the 1.26 – 1.71 μm region for planetary investigations (T = 80 – 300 K). Application to Titan. Icarus, 219, 110 – 128.

Conrath, B.J., Gierasch, P.J., Ustinov, E.A., 1998. Thermal structure and para hydrogen fraction on the outer planets from Voyager IRIS measurements. Icarus 135, 501 – 517.

Cushing, M.C., Vacca, W.D., Rayner, J.T. 2004. Spextool: A spectral extraction package for SpeX, a 0.85.5 micron cross-dispersed spectrograph. Publ. of Ast. Soc. Pacific, 116, 362 – 376.

Cutri, R.M. et al. 2003. 2MASS All Sky Catalog of point sources. The IRSA 2MASS All-Sky Point Source Catalog, NASA/IPAC Infrared Science Archive.

de Pater, I., Fletcher, L.N., Luszcz-Cook, S., DeBoer, D., Butler, B., Hammel, H B., Sitko, M.L., Orton, G., Marcus, P.S. 2014. Neptune's global circulation deduced from multi-wavelength observations. Icarus, 237, 211 – 238.

de Pater, I., Sromovsky, L. A., Fry, P. M., Hammel, H B., Baranec, C., Sayanagi, K.M., 2015. Record-breaking storm activity on Uranus in 2014. Icarus, 252, 121 – 128.

Fiorenza, C., Formisano, V., 2005. A solar spectrum for PFS data analysis. Plan. Space Sci. 53, 1009 – 1016.

Fletcher, L.N., Hesman, B.E., Achterberg, R.K., Irwin, P.G.J., Bjoraker, G., Gorius, N., Hurley, J., Sinclair, J., Orton, G.S., Legarreta, J., Garcia-Melendo, E., Sánchez-Lavega, A., Read, P.L., Simon-Miller, A.A., Flasar, F.M., 2012. The origin and evolution of Saturns 2011-2012 stratospheric vortex. Icarus, 221, 560 – 586.

Fletcher, L.N., Hesman, B.E., Irwin, P.G.J., Baines, K.H., Momary, T.W., Sánchez-Lavega, A., Flasar, F.M., Read, P.L., Orton, G.S., Simon-Miller, A., Hueso, R., Bjoraker, G.L., Mamoutkine, A., del Rio-Gaztelurrutia, T., Gomez, J.M., Buratti, B., Clark, R.N., Nicholson, P.D., Sotin, C., 2011. Thermal Structure and Dynamics of Saturn's Northern Springtime Disturbance. Science, 332, 1413 – 1417.

Fouchet, T., Lellouch, E., Feuchtgruber, H., 2003. The hydrogen ortho-to-para ratio in the stratospheres of the giant planets. Icarus, 161, 127 – 143.

Hammel, H.B., Rages, K., Lockwood, G.W., Karkoschka, E., de Pater, I. 2001. New measurements of the winds on Uranus. Icarus, 153, 229 – 235.

Hartmann, J.-M., Boulet, C., Brodbeck, C., van Thanh, N., Fouchet, T., Drossart, P., 2002. A far wing lineshape for H_2 broadened CH_4 infrared transitions. J. Quant. Spec. Radiat. Transf., 72, 117 – 122.

Irwin, P.G.J., Teanby, N.A., de Kok, R., Fletcher, L.N., Howett, C.J.A., Tsang, C.C.C., Wilson, C.F., Calcutt, S.B., Nixon, C.A., & Parrish, P.D., 2008. The NEMESIS planetary atmosphere radiative transfer and retrieval tool. J. Quant. Spec. Radiat. Transf., 109, 1136 – 1150.

Irwin, P.G.J., de Bergh, C., Courtin, R., Bézard, B., Teanby, N.A., Davis, G.R., Fletcher, L.N., Orton, G.S., Calcutt, S.B., Tice, D.S., & Hurley, J. 2012. The application of new methane line absorption data to Gemini-N/NIFS and KPNO/FTS observations of Uranus' near-infrared spectrum. Icarus, 220, 369 – 382.

Irwin, P.G.J., Tice, D.S., Fletcher, L.N., Barstow, J.K., Teanby, N.A., Orton, G.S. & Davis, G.R., 2015. Reanalysis of Uranus' cloud scattering properties from IRTF/SpeX observations using a self-consistent scattering cloud retrieval scheme. Icarus, 250, 462 – 476.

Karkoschka, E., Tomasko, M., 2009. The haze and methane distributions on Uranus from HSTSTIS spectroscopy. Icarus, 202, 287 – 302.

Lacis, A.A., Oinas, V., 1991. A description of the correlated-k distribution method for modelling nongray gaseous absorption, thermal emission, and multiple scattering in vertically inhomogeneous atmospheres. J. Geophys. Res., 96, 9027 – 9063.

Martonchik, J.V., Orton, G.S., 1994. Optical constants of liquid and solid methane. Appl. Opt. 33, 8306 – 8317.

Orton, G.S., Fletcher, L.N., Encrenaz, T., Leyrat, C., Roe, H.G., Fujiyoshi, T., Pantin, E., 2015. Icarus, submitted.

Sánchez-Lavega et al. 2011. Deep winds beneath Saturns upper clouds from a seasonal long-lived planetary-scale storm. Nature, 475, 71 – 74.

Sromovsky, L.A., Fry, P.M., Hammel, H.B., de Pater, I., Rages. K.A., Showalter, M.R., 2007. Dynamics, evolution and structure of Uranus' brightest cloud feature. Icarus192, 558 – 575.

Sromovsky, L.A., Fry, P.M., Hammel, H.B., Ahue. W.M., de Pater, I., Rages. K.A., Showalter, M.R., van Dam, M.A., 2009. Uranus at equinox: Cloud morphology and dynamics. Icarus203, 265 – 286.

Sromovsky, L.A., Fry, P.M., Kim, J.H., 2011. Methane on Uranus: The case for a compact CH4 cloud layer at low latitudes and a severe CH_4 depletion at high latitudes based on a re-analysis of Voyager occultation measurements and STIS spectroscopy. Icarus215, 292 – 312.

Sromovsky, L.A., Hammel, H.B., de Pater, I., Fry, P.M., Rages. K.A., Showalter, M.R., Merline, W.J., Tamblyn, P., Neyman, C., Margot, J.-L., Fang, J., Colas, F., Dauvergne, J.,-L., Gomez-Forrellad, J.M., Hueso, R., Sanchez-Lavega, A., Stallard, T., 2012. Episodic bright and dark spots on Uranus. Icarus, 220, 6 – 22.

Tice, D.S., Irwin, P.G.J., Fletcher, L.N., Teanby, N.A., Hurley, J., Orton, G.S., Davis, G.R., 2013. Uranus' cloud particle properties and latitudinal methane variation from IRTF SpeX observations. Icarus, 223, 684 – 698.

Vacca, W.D., Cushing, M.C., Rayner, J.T. 2003. A Method of Correcting Near-Infrared Spectra for Telluric Absorption. Publ. of Ast. Soc. Pacific, 115, 389 – 409.

Zheng, C., Borysow, A., 1995. Modeling of collision-induced infrared absorption spectra of H_2 pairs in the first overtone band at temperatures from 20 to 500 K. Icarus, 113, 84 – 90.

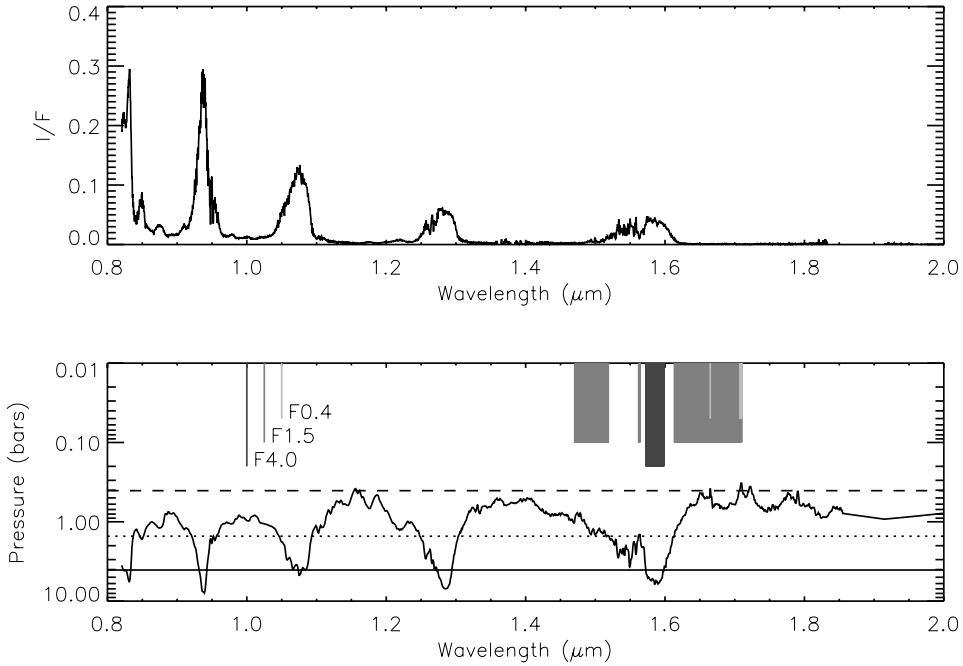

Fig. 1.— Top panel shows a typical I/F spectrum of Uranus as observed by IRTF/SpeX. Bottom panel shows the pressure level in Uranus' atmosphere at which the transmission to space is 0.5. Overplotted in the bottom panel are the chosen cut-off pressures of 4, 1.5 and 0.4 bar. Continuum images ('F4.0') are averaged over all wavelengths where the transmission to 4 bars exceeds 0.5. Medium-absorption and high-absorption images are averaged over all wavelengths where the transmission at 1.5 and 0.4 bars is respectively **less** than 0.5, labelled respectively as 'F1.5' and 'F0.4'. The wavelengths selected by these filters in the wavelength range modelled (1.47 – 1.71 μm) are indicated by the grey regions in the bottom panel of differing length and darkness; a key to these filter regions is indicated by the vertical bars in the top left of the bottom panel.

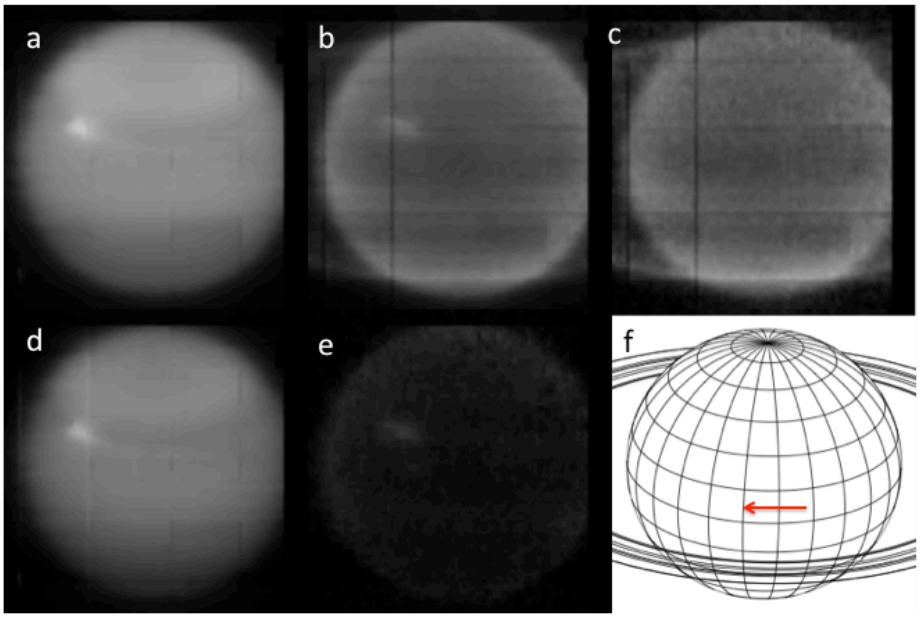

Fig. 2.— Average of observations made on 31^{st} October 2014 between 01:42 and 02:17 (UT). These images are the averaged mosiacs of all observed frames, where overlap between the frames creates the small striations seen. Uranus' north pole is at the top. The top row shows the appearance of Uranus in the different wavelength 'filters'. Panel (a) shows the planet at wavelengths where the transmission to space exceeds 0.5 at the 4-bar level (i.e. the 'F4.0' filter). Panel (b) shows the planet at wavelengths where the transmission to the 1.5 bar level is less than 0.5 ('F1.5'), while panel (c) shows the planet at wavelengths where the transmission to the 0.4 bar level is less than 0.5 ('F0.4'), which is only sensitive to the hazes at pressures less than 0.2 bar. Uranus' epsilon-ring is visible in panels (b) and (c). The bottom row shows differences between the images to highlight the clouds at different levels. Panel (d) shows panel (a) minus panel (b) and shows the distribution of cloud reflectivity of the cloud decks at pressures $>\sim$ 1 bar, while panel (e) shows panel (b) minus panel (c), showing the distribution of clouds roughly between 1 and 0.2 bar. Panel (f) shows a projection of Uranus' disc and rings for reference. Uranus' sense of rotation is indicated by the arrow in panel (f).

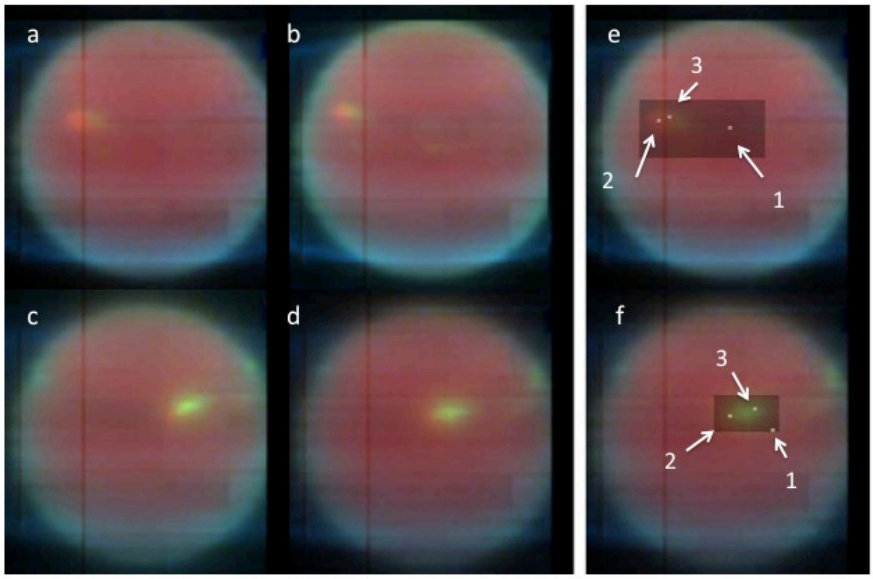

Fig. 3.— False colour summary of observations. Observations of 31^{st} October 2014 are on the top row, with panel (a) showing the average between 01:42 – 02:17 and panel (b) showing the average from 02:21 – 02:56 (UT), when the storm cloud is closer to the evening limb. In these false-colour images, red is the continuum F4.0 image (i.e. panel (a) in Fig.2), green is the F1.5 image where $\mathrm{Trans}_{1.5bar} < 0.5$ (i.e. panel (b) in Fig.2) and blue is the F0.4 image where $\mathrm{Trans}_{0.4bar} < 0.5$ (i.e. panel (c) in Fig.2). In this scheme, deep clouds appear red, intermediate clouds appear yellow and high hazes appear bluish. Observations on 11^{th} November 2014 are shown on the bottom row, with panel (c) showing the average between 00:36 – 01:12, when the storm is nearer the morning limb and panel (d) showing the average from 01:15 – 01:50 (UT). It can be seen that the centre of the deep cloud is offset from the centre of the cloud between 1 and 0.2 bar since the deep 'red' cloud is consistently seen to the left of the overlying 'yellow' cloud. The right hand panels (e) and (f) reproduce panels a) and d), respectively, and indicate where spectra were extracted and analysed for the nights of 31^{st} October 2014 and 11^{th} November 2014. Individual points are indicated, while the greyed areas indicate the regions mapped in our area retrievals, shown later in Figs.11 – 14.

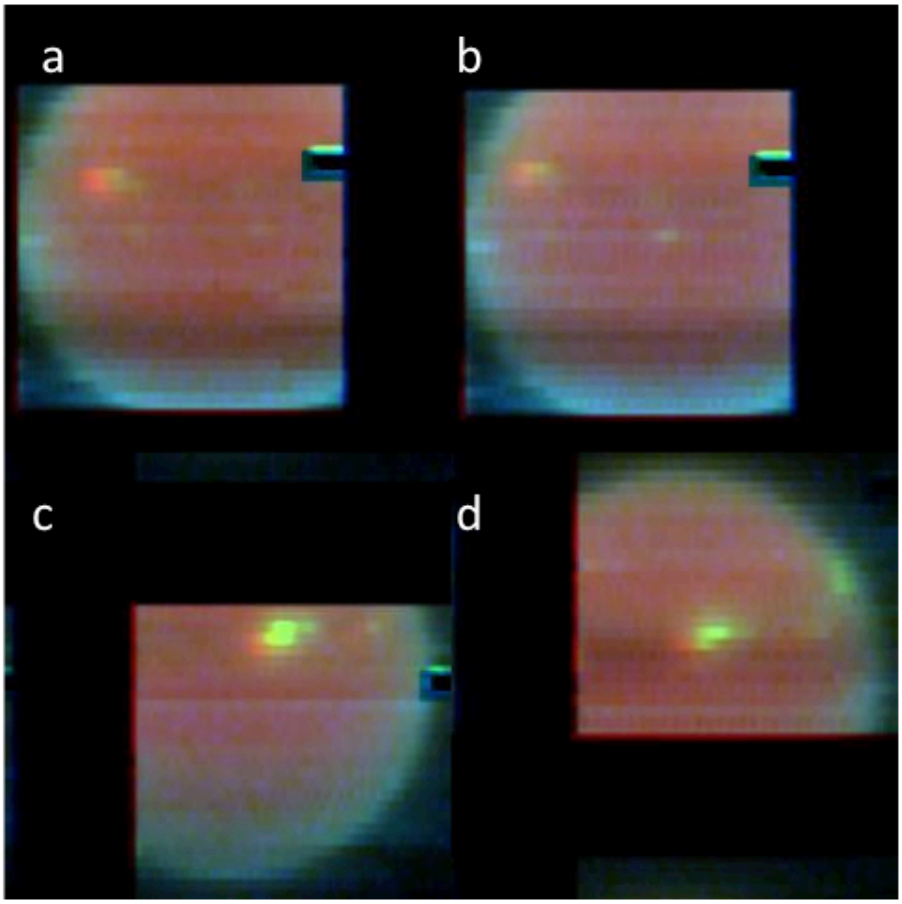

Fig. 4.— As for Fig.3, except here we have used individual frames taken in the same observation blocks, to mitigate the smearing effect introduced by Uranus' rotation at the expense of reduced SNR. The increased brightness of the upper level clouds between 1.5 and 0.2 bars on 11^{th} November 2014 is clear, as is the offset between the deep and upper components of the cloud feature.

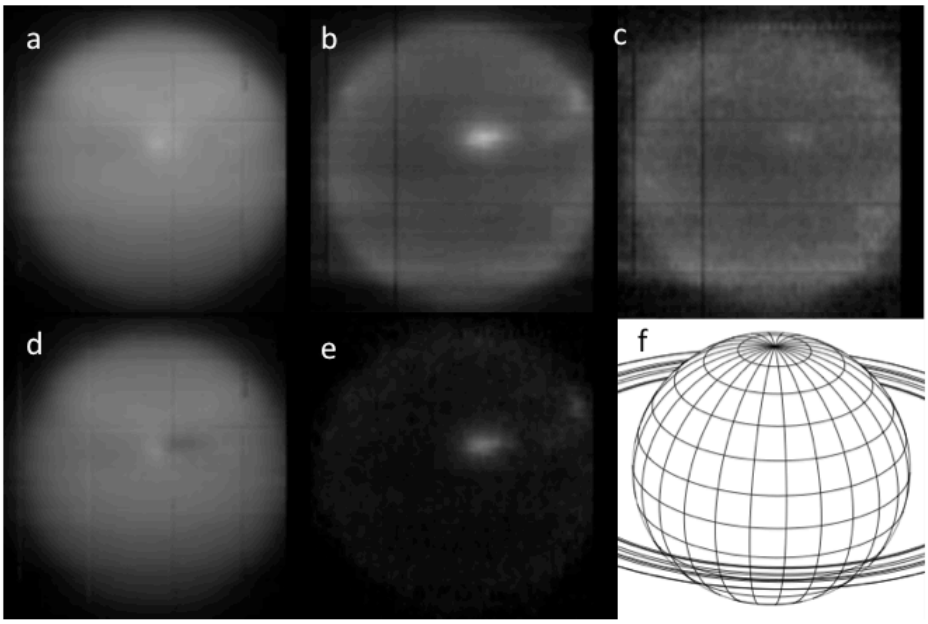

Fig. 5.— As Fig.2, but showing the average of observations made on 11^{th} November 2014 between 01:15 and 01:50 (UT). The same brightness levels have been used in plotting these images and it can be seen that the cloud between the ~ 1 and 0.2 bar levels is brighter here than on 31^{st} October 2014. The cloud can also be seen faintly in panel (c), showing that the cloud really has reached a higher altitude than it had achieved on 31^{st} October.

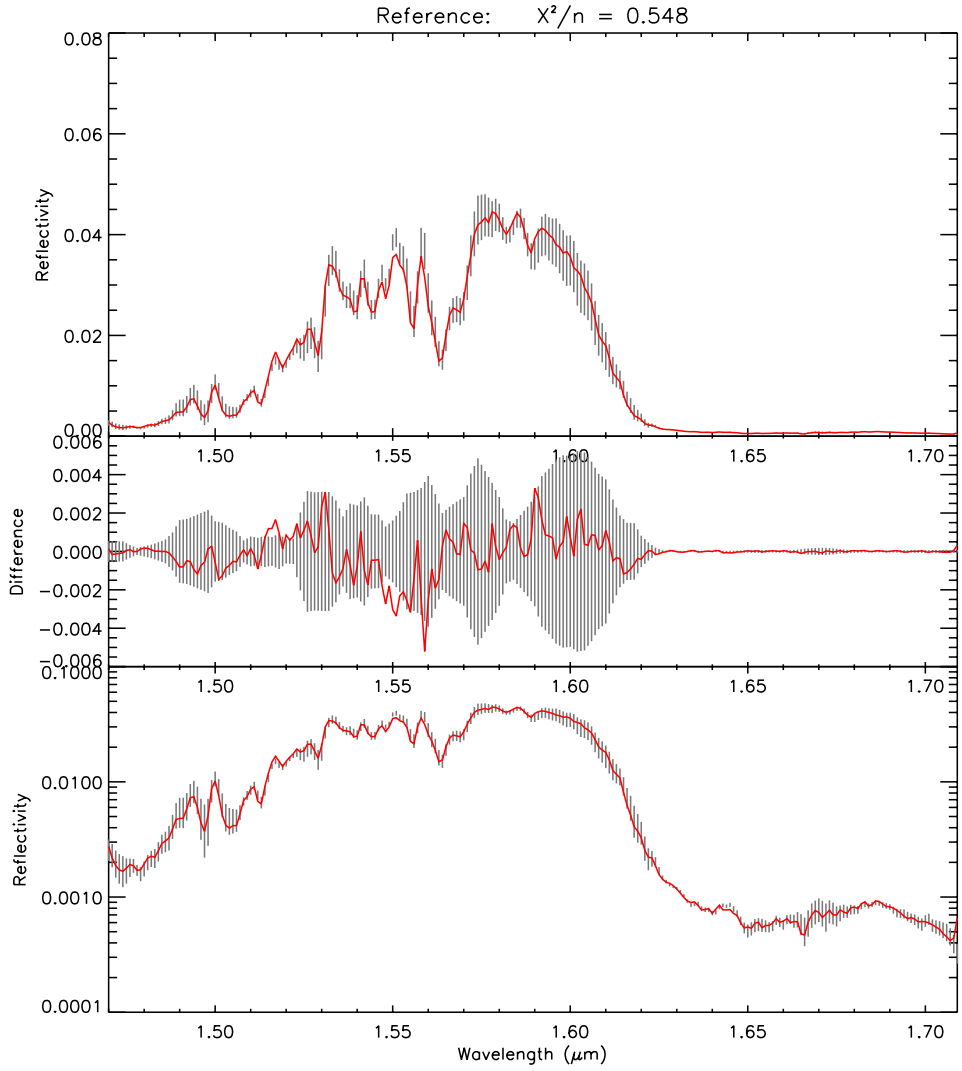

Fig. 6.— Observed and fitted spectrum at reference point 1, well away from the storm cloud on 31^{st} October 2014. Top panel compares the measured (black with error bars) and modelled spectra (red line) , the middle panel shows the difference between the measured and modelled spectra (red line) compared with the error bars, while the bottom panel compares the measured and modelled spectra on a log scale to highlight the low reflectivity regions.

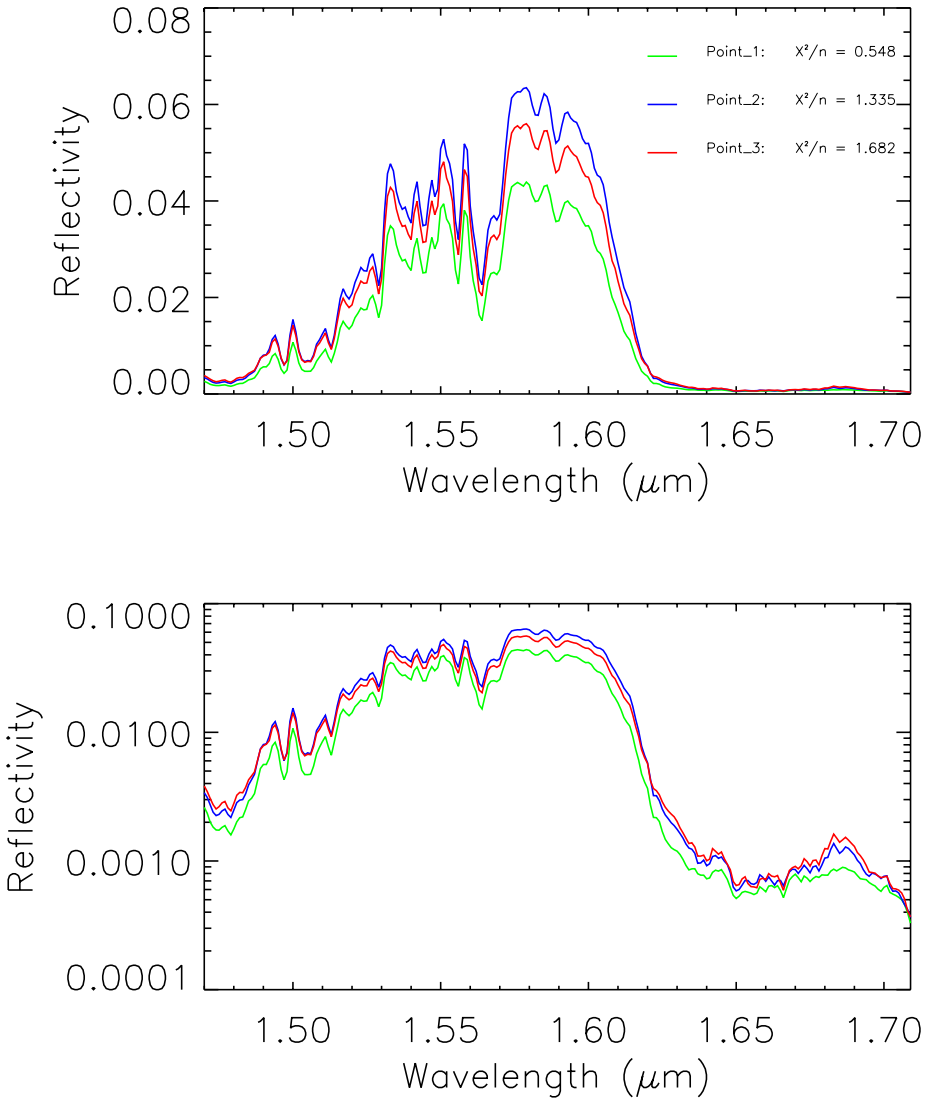

Fig. 7.— Comparison of the measured spectra for the three sample points on 31^{st} October 2014, indicated in Fig.3: (1) reference point well away from storm; (2) middle of deeper cloud feature; (3) middle of upper cloud feature. The top panel shows the reflectivity spectrum in linear units, while the bottom panel shows log(reflectivity) to accentuate the strongly absorbing spectral regions. The χ^2/n values in the top panel indicate the closeness of fit that could be achieved to these three spectra with our NEMESIS retrieval model.

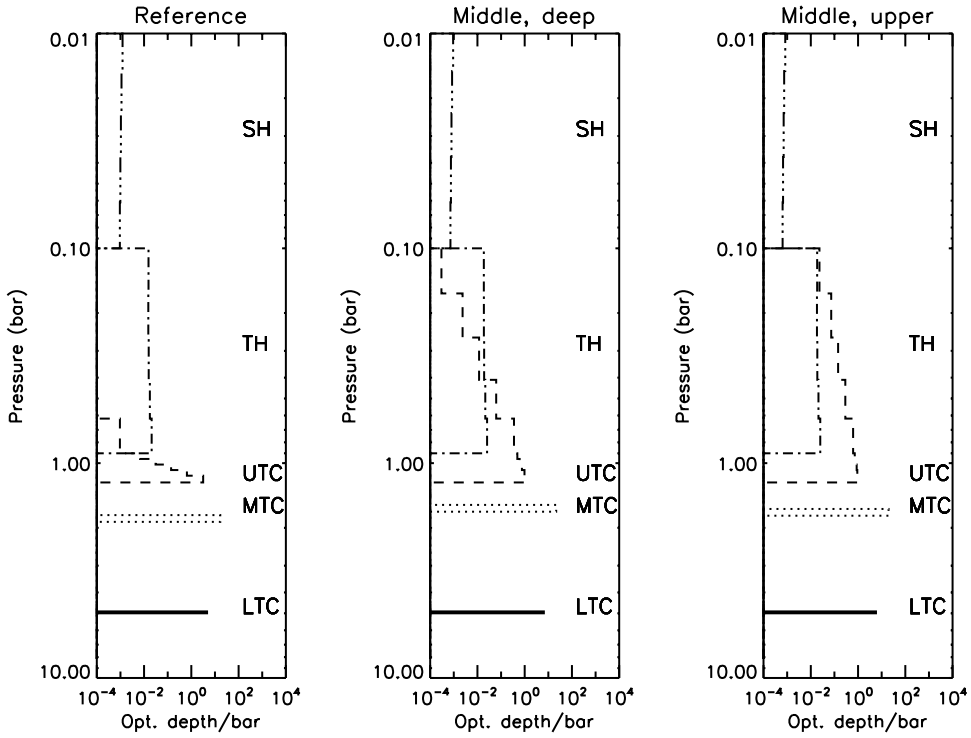

Fig. 8.— Comparison of the three fitted cloud profiles retrieved from the three test points on 31^{st} October 2014: (1) reference point well away from storm; (2) middle of deeper cloud feature; (3) middle of the upper cloud feature. Optical depths are quoted at a wavelength of 1.6 μm.

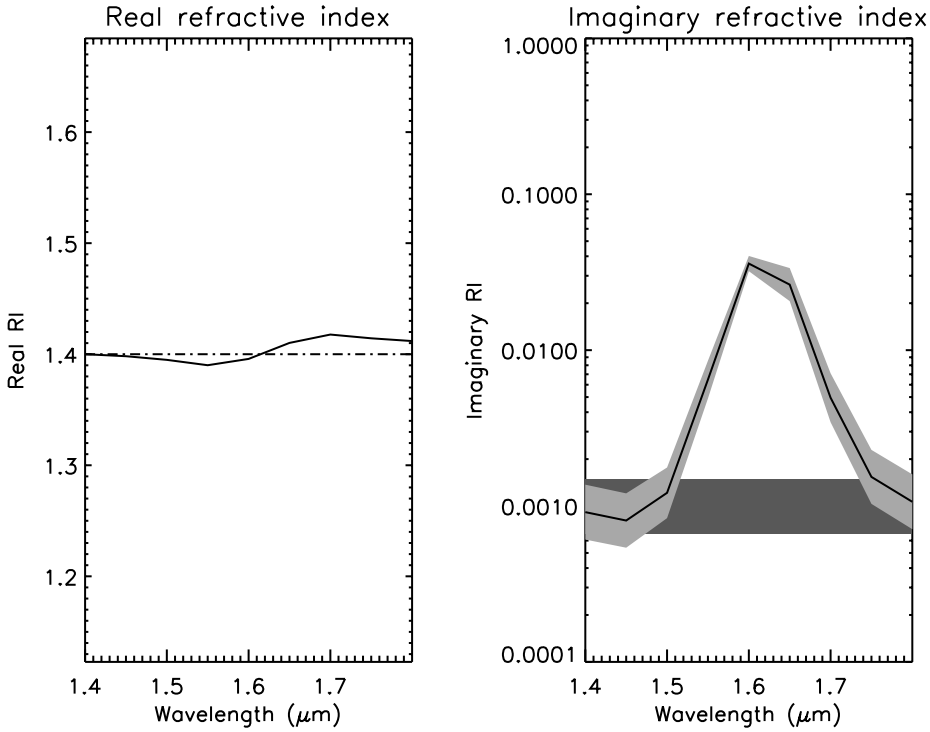

Fig. 9.— Retrieved refractive index spectra of the Middle Tropospheric Cloud (MTC) at 2–3 bars for case 1 of the 31^{st} October 2014 test retrievals, showing adjustment necessary to properly fit the long-wave edge of the 1.57 μm peak. Very similar refractive index spectra were derived at all points. In the left hand panel the a priori real refractive index spectrum is the dot-dash line, while the fitted spectrum is the solid line. In the right hand panel, the a priori imaginary refractive index and errors are indicated by the dark grey region, while the fitted spectrum is shown by the solid line, with errors indicated in light grey.

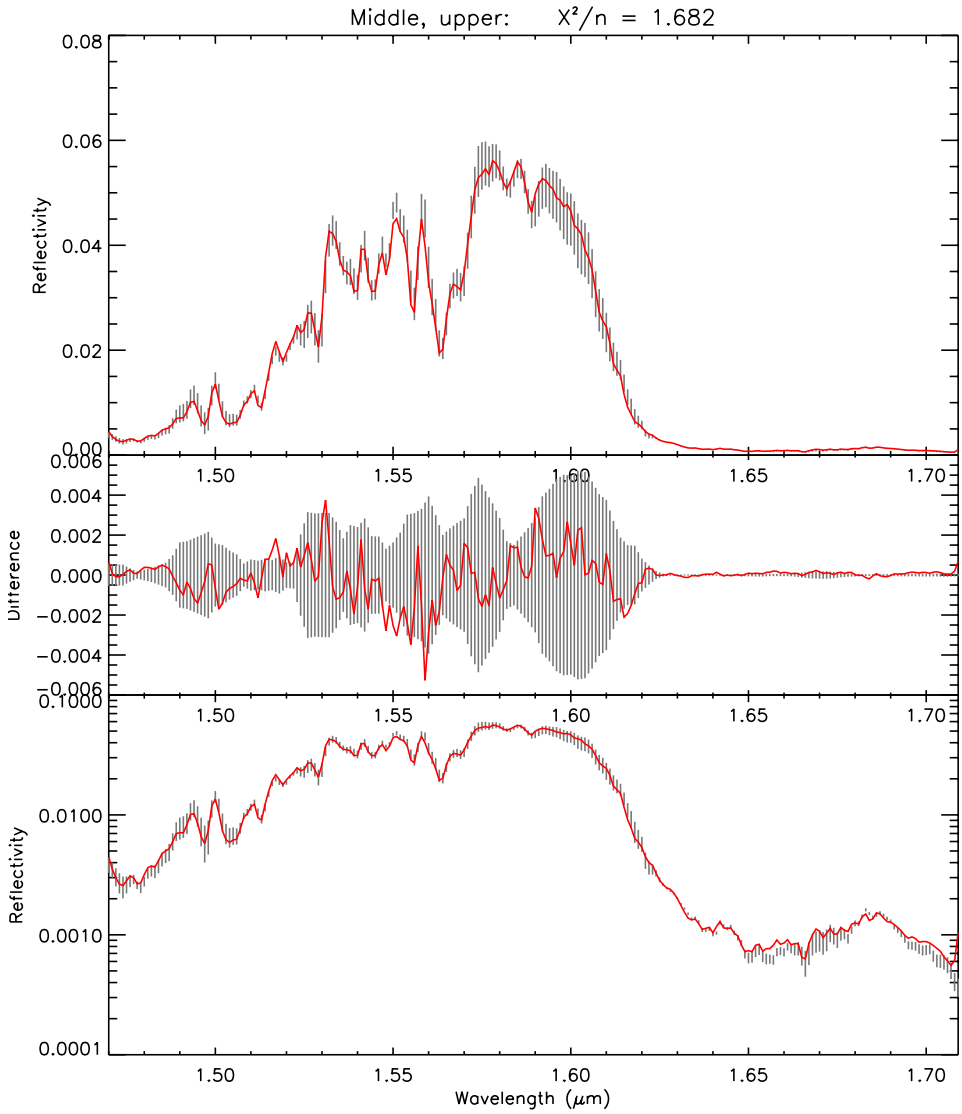

Fig. 10.— As Fig.6, except for point 3 of the 31^{st} October 2014 test retrievals (indicated in Fig.3), in the middle of the higher cloud where our fit is poorest, showing that we still achieve an acceptable fit between the modelled and measured spectra.

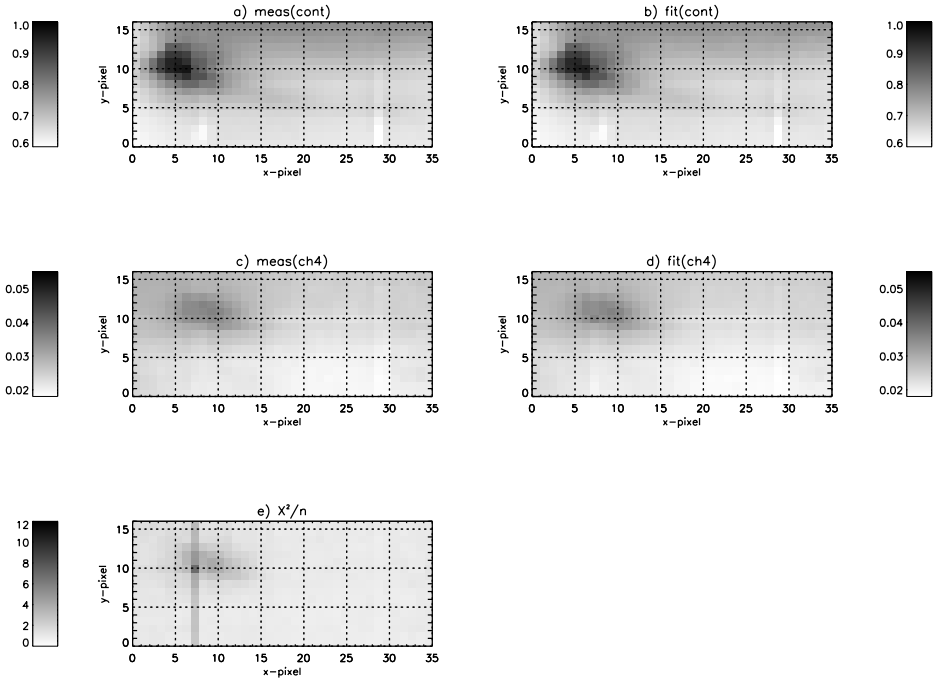

Fig. 11.— Observed and fitted radiances in the continuum (average of 1.55 – 1.62 μm, top row, panels a) and b)) and medium methane absorption (average of 1.62 – 1.65 μm, middle row, panels c) and d)) bands together with the variation of χ^2/n for first set of 31^{st} October observations (bottom, panel e)). Radiance units are μW cm^{-2} sr^{-1} μm^{-1}. The area covered by these retrievals is indicated in Fig.3.

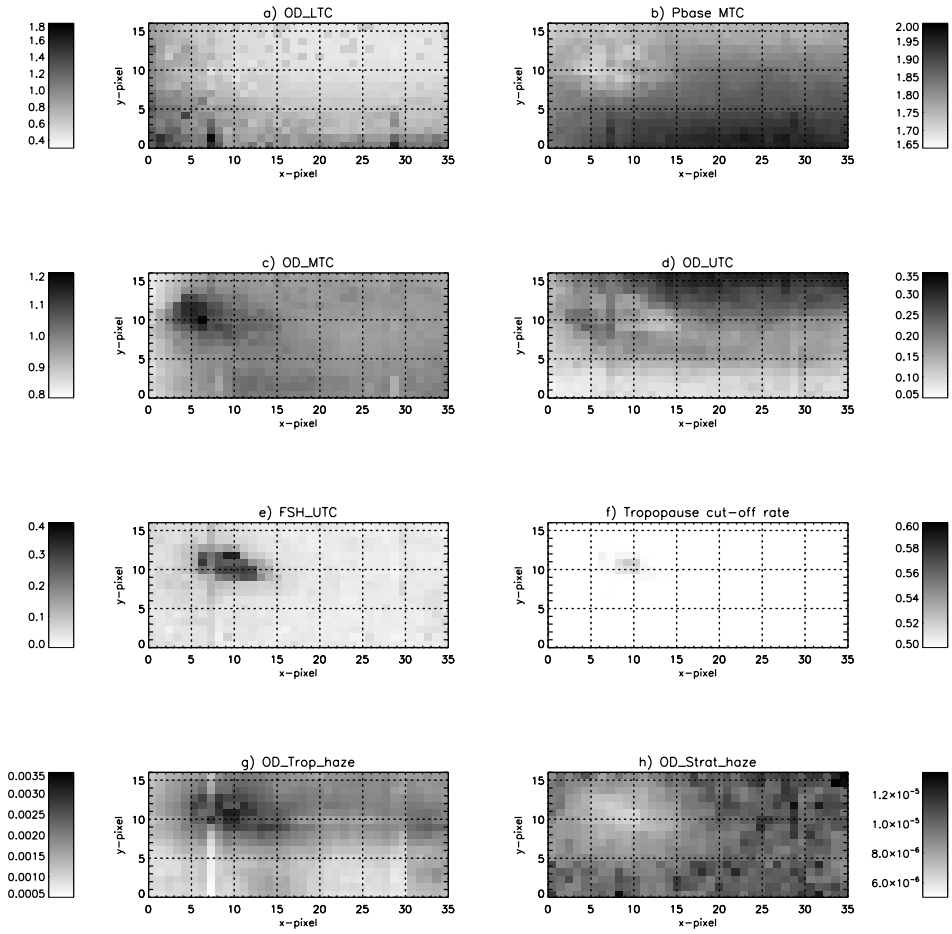

Fig. 12.— Fitted cloud parameters for first set of 31^{st} October observations. Panels are: a) opacity (at 1.6 μm) of the Lower Tropospheric Cloud (OD-LTC); b) base pressure of Middle Tropospheric Cloud (Pbase MTC); c) opacity of the MTC (OD-MTC); d) opacity of the Upper Tropospheric Cloud (OD-UTC); e) Fractional scale height of UTC (FSH-UTC); f) Tropopause cut-off parameter, α; g) opacity of Tropospheric Haze (OD-Trop-haze); and h) opacity of Stratospheric Haze (OD-Strat-haze)

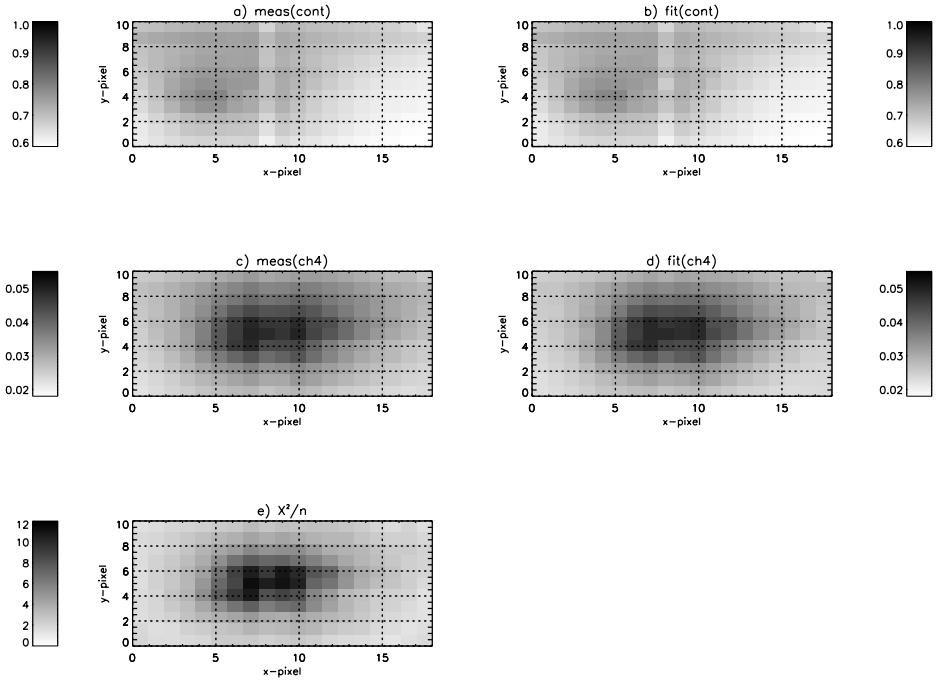

Fig. 13.— As Fig.11, but showing observed and fitted radiances in the continuum (average of 1.55 – 1.62 μm) and medium methane absorption (average of 1.62 – 1.65 μm) bands together with the variation of χ^2/n for storm region for second set of 11^{th} November observations.

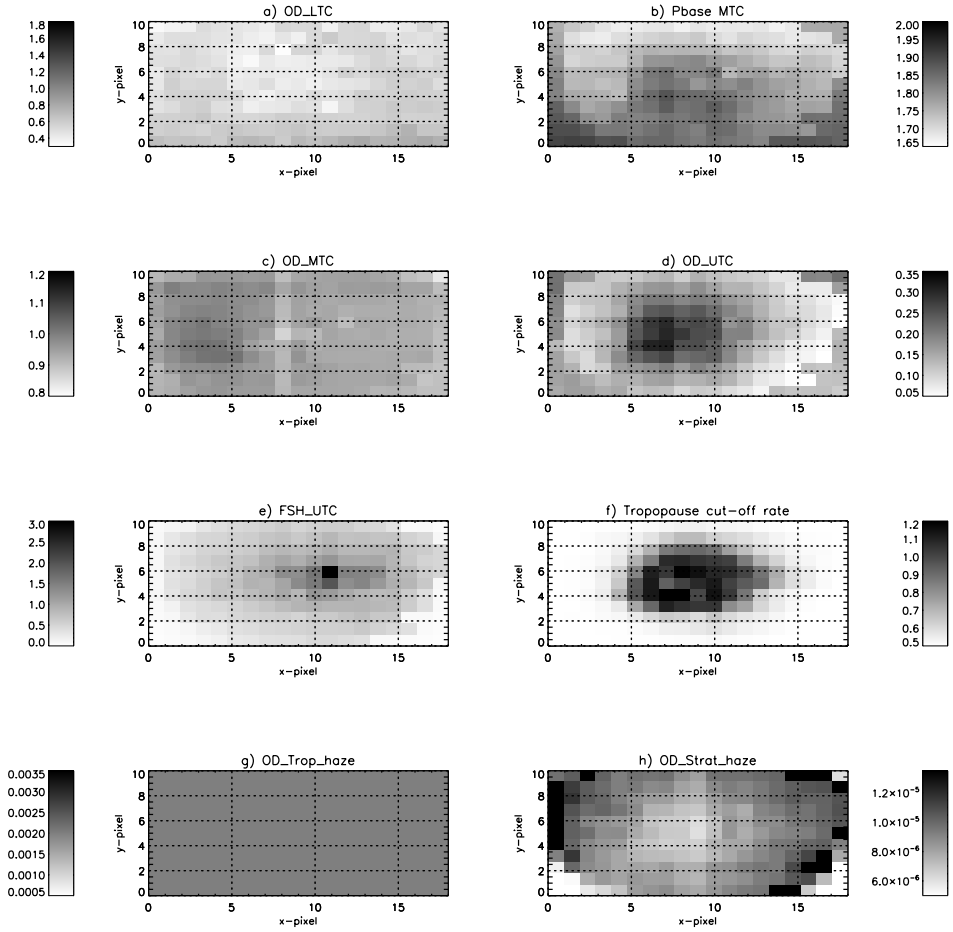

Fig. 14.— As Fig.12, but showing the fitted cloud parameters for storm region for second set of 11^{th} November observations. Note here that the opacity of the TH was fixed to 0.002 to prevent the retrieval becoming unstable.

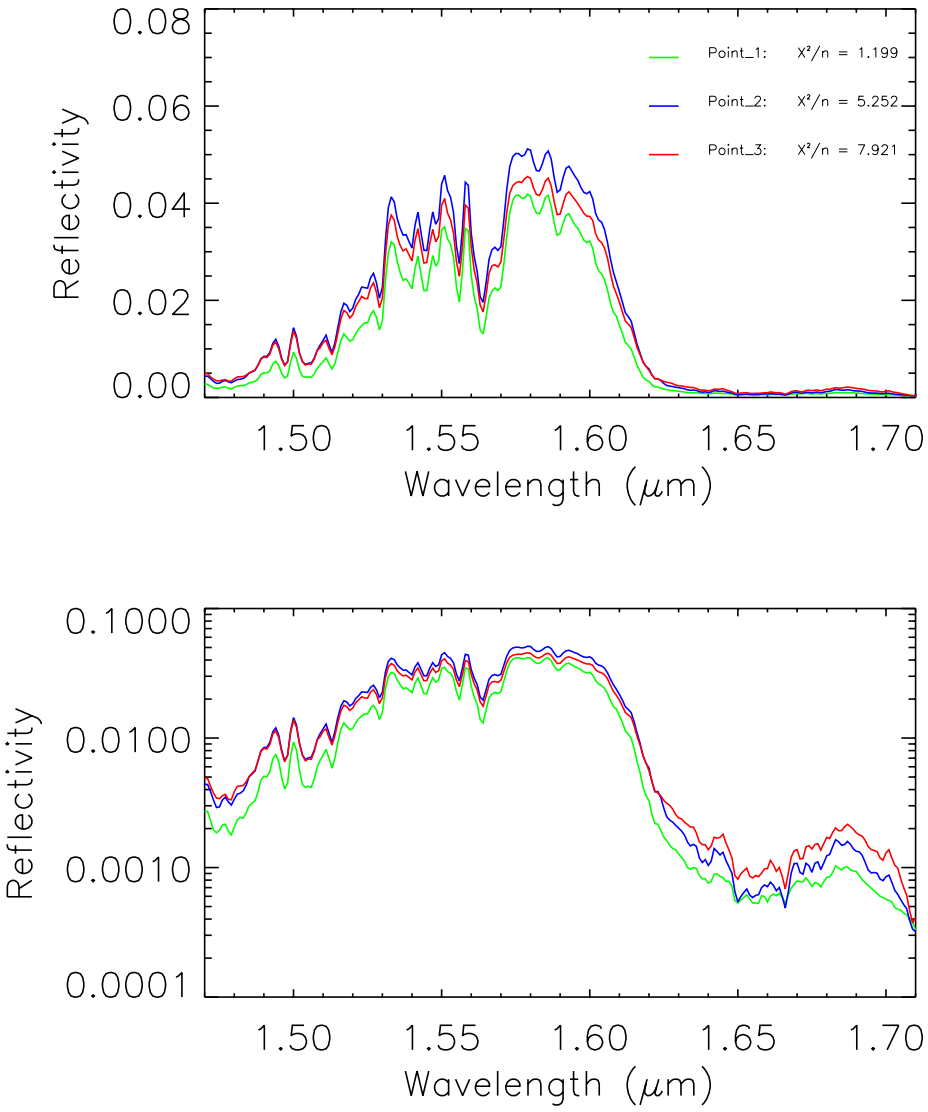

Fig. 15.— As Fig.7, but showing a comparison of the three sample observed spectra for 11^{th} November indicated in Fig.3: (1) reference point away from storm; (2) middle of deeper cloud feature; (3) middle of upper cloud feature.

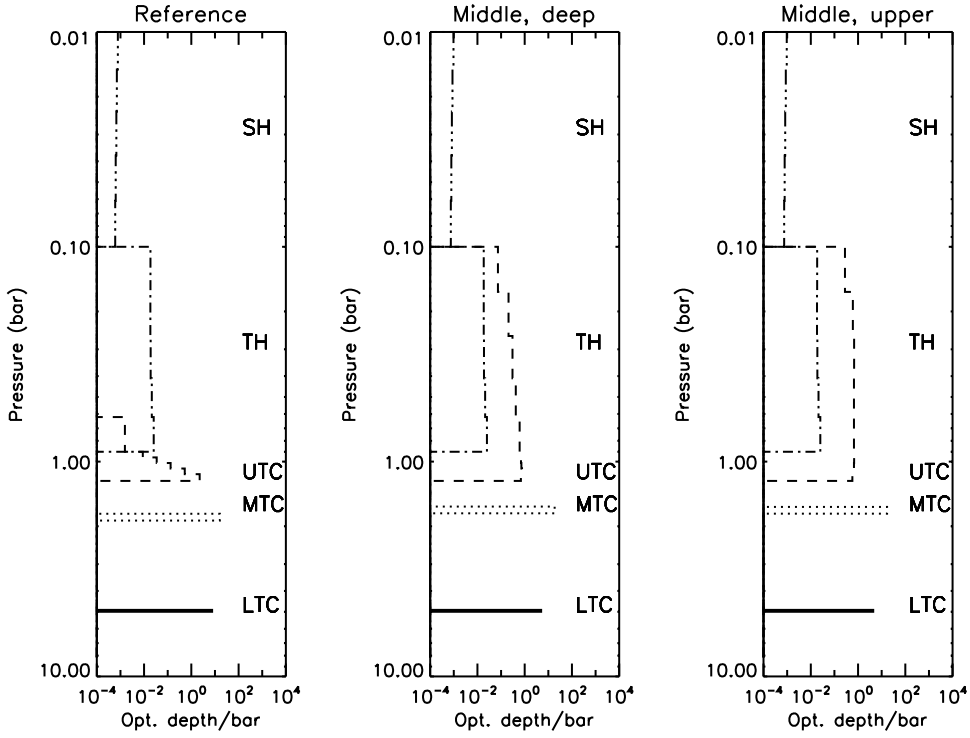

Fig. 16.— As Fig.8, but showing a comparison of three fitted cloud profiles for 11^{th} November: (1) reference point away from storm; (2) middle of deeper cloud feature; (3) middle of upper cloud feature. The similarity in the vertical distribution of the UTC and TH for case 3 leads to the TH opacity becoming indistinguishable from the UTC parameters at pixels near the centre of the upper level cloud, causing the instability that forced us to fix the TH opacity in the 11^{th} November retrievals.

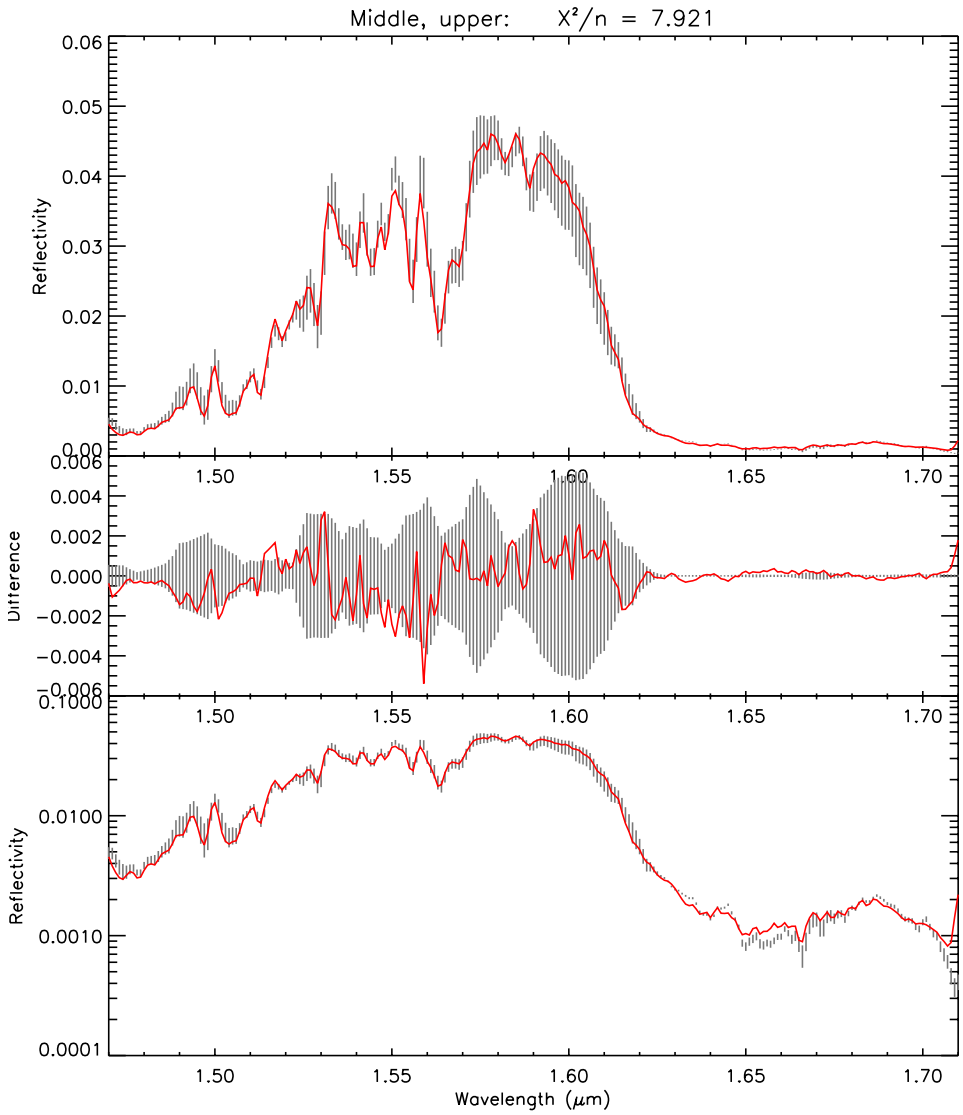

Fig. 17.— As Fig.10, but comparing the observed and fitted spectrum at point 3 in the middle of the upper cloud feature for 11^{th} November, where our fit is poorest.

Table 1. 2014 VLT/SINFONI Observations.

Date	T_{start} (UT)	T_{end} (UT)	Grism	N_{exp}[a]	T_{exp}	NDIT	Plate Scale
31^{st} October 2014	01:42	02:17	H	24	60s	1	0.1″
31^{st} October 2014[b]	02:21	02:56	H	24	60s	1	0.1″
11^{th} November 2014	00:36	01:12	H	24	60s	1	0.1″
11^{th} November 2014	01:15	01:50	H	24	60s	1	0.1″

[a]The observation sequence combined four sets of observations, in which for each there were five planet observations (2× 2 mosaic plus once in the centre) and one sky observation.

[b]Observations were also made November 8^{th} and 9^{th} 2014 during poorer weather conditions, but these are of too low quality to present here.